Crustal structure of Eritrea from receiver function analysis

M. Gauntlett[1], S. N. Stephenson[1], J-M. Kendall[1], C. Ogden[2], J. Hammond[3], B. Goitom[4], G. Ogubazghi[5]

[1]Department of Earth Sciences, University of Oxford, UK
[2]School of Geography, Geology and the Environment, University of Leicester, UK
[3]Department of Earth and Planetary Sciences, Birkbeck, University of London, UK
[4]School of Earth Sciences, University of Bristol, UK
[5]Eritrea Institute of Technology, Eritrea

Key Points:

- Receiver functions produce the first estimates of Eritrean bulk crustal properties
- Eritrean crust is denser than global average and highly heterogeneous
- Evidence found for melt within crust and for regional sub-crustal support from hotter mantle

Corresponding author: Miriam Gauntlett, `miriam.gauntlett@linacre.ox.ac.uk`

Abstract

Located near the Afar Triple Junction, Eritrea hosts the Danakil microplate and is undergoing the final stages of on-land rifting. To better understand the nature of the Eritrean crust and continental breakup, we calculate teleseismic receiver functions across Eritrea and Afar. We estimate the Moho depth and bulk crustal V_P/V_S ratio using the H-κ stacking method. The heterogeneity of our crustal thickness results ($\sim$35 km — $\sim$19 km) indicates that the Danakil microplate has undergone stretching and crustal thinning, and that rifting is highly localised in the Gulf of Zula. By investigating the relationship between crustal thickness and topographic elevation in Eritrea and Afar, we estimate the regional crustal density as $\rho_c \approx 2950$ km m^{-3}, which is denser than the global average of $\rho_c \approx 2880$ kg m^{-3}. Our results demonstrate very strongly positive residual topography in the region. We propose that this topography is supported by the mantle plume responsible for the onset of rifting in East Africa, generating uplift due to the presence of a hot thermal anomaly beneath the plate and by thinning of the lithospheric mantle. We also observe high V_P/V_S ratios of > 1.9 in Eritrea. Our results demonstrate the presence of partial melt in the crust, and that magma-assisted extension continues to be important in the final stages of continental breakup.

Plain Language Summary

Eritrea and surrounding regions host three tectonic plate boundaries that are pulling apart from one another (rifting) as continental breakup is occurring. These rifting processes have led to a complicated tectonic history. To better understand the nature of the Eritrean crust, we study seismic data to produce estimates of crustal thickness and the ratio of seismic wave speeds. Our results indicate that the crust beneath Eritrea shows substantial variation in thickness, meaning that the Danakil has undergone crustal thinning. We observe a denser crust in Eritrea than the global average. The ground elevation in Eritrea is anomalously high for the observed thicknesses of Eritrean crust, implying that the hotter mantle plays a role in supporting the elevation. We also show that partially molten rock (magma) is likely to be present under certain parts of the country, which is evidence that magma assists with continental breakup.

1 Introduction

The East African Rift System is an ideal setting to investigate the temporal and spatial evolution of continental rifting. It consists of a network of rifts that developed asynchronously and are simultaneously undergoing different stages of the rifting process. Initial continental breakup is occurring in the south of the EARS in Mozambique, while further to the north, full seafloor spreading has been established in the Gulf of Aden and the Red Sea (e.g., Manighetti et al., 1998; Tesfaye et al., 2003). Elsewhere, the Main Ethiopian Rift shows the intermediate stages of more developed continental rifting, while Afar is undergoing the final stages of continental breakup as it develops into oceanic rifting in the transitional Red Sea zone (e.g., Makris & Ginzburg, 1987; Kogan et al., 2012). It is currently a matter of debate whether full sea floor spreading has begun on land in Afar.

The Afar region is a diffuse extensional province which hosts a triple junction formed by the meeting of three diverging plate boundaries: the Main Ethiopian Rift, the Gulf of Aden and the Red Sea, separating the Nubian, Somalian and Arabian tectonic plates respectively. The Gulf of Aden and the Red Sea do not directly connect in Afar, but are actively propagating through the region via the development of a series of disconnected, propagating rift segments (e.g., Manighetti et al., 1998). Instead of directly connecting to the Gulf of Aden through the Bab el-Mandeb Strait, the Red Sea bifurcates into two branches south of 16°N (Barberi & Varet, 1977). This process has isolated the Danakil microplate, a sliver of continental crust rotating independently of Nubia (Sichler, 1980;

Viltres et al., 2020). The exact boundaries of the Danakil block are not well-constrained. Due to its remote location, very few studies have been undertaken in the region, meaning there is a lack of information on the microplate and its role in partitioning strain between the two branches of the Red Sea Rift.

The nature of the crust beneath Afar has been widely debated by researchers. Some studies claim new oceanic crust is being created in the region (e.g., Mohr, 1989), whilst others conclude that the area is entirely underlain by intruded, stretched continental crust (e.g., Makris & Ginzburg, 1987). An alternative proposal is that the overall crustal composition is transitional between continental and oceanic. The region west of the current rift axis is predominantly made up of mafic material with oceanic affinities, whereas continental material exists to the east, potentially connected to the Danakil block (e.g., Redfield et al., 2003; Hammond, Kendall, et al., 2011).

Continental breakup involves extensional faulting, ductile plate stretching and intrusive and extrusive magmatism (e.g., Barton & White, 1997; White & McKenzie, 1989; Bastow & Keir, 2011). It is crucial to elucidate the extent to which mechanical or magma-assisted extension processes dominate at each stage of continental breakup as it transitions into seafloor spreading. Indeed, this transition process may be more complex than a smooth evolution from mechanical to magma-dominated extension into oceanic spreading. Previous studies in the East African Rift system have shown that upper-crustal extension throughout much of Ethiopia is accommodated primarily by dyke intrusion along narrow, magmatic segments, i.e., it has migrated away from the border faults and localised to rift-aligned magmatic intrusions (e.g., Ebinger & Casey, 2001; Wolfenden et al., 2004). However, the Danakil Depression to the north, which has been affected by magmatism since rift onset, now hosts markedly thinned continental crust, coupled with marked subsidence and thick evaporite deposition (Hutchinson & Engels, 1972; Wolfenden et al., 2005; Keir et al., 2013). Thus, it has been proposed that the final stages of breakup in Ethiopia may be characterised by a return to ductile plate stretching and upper-crustal brittle faulting (Bastow et al., 2018).

Hammond, Kendall, et al. (2011) comment that the lack of data from Eritrea limits its overall regional interpretations of crustal structure. Eritrea hosts the northern part of the Ethiopian Plateau, the Gulf of Zula, the Danakil Depression, the Danakil Alps and substantial off-rift volcanism in the Nabro Volcanic Range. The strike of the Nabro Volcanic Range is almost parallel to the trend of the Hanish-Zukur islands in the Red Sea and perpendicular to regional Red Sea rift trends. The presence of these volcanic centers across the Danakil block has led to proposals that they represent the surface expression of a 'leaky' transform fault accommodating strain transfer from the Red Sea into Afar (e.g., Barberi & Varet, 1977; Viltres et al., 2020).

Crustal thickness and the ratio of P-wave velocity to S-wave velocity (V_P/V_S ratio) provide key constraints on crustal composition and the amount of partial melt hosted by the crust (e.g., Zandt & Ammon, 1995; Dugda et al., 2005; Stuart et al., 2006). Previous studies of crustal structure in the region have shown that the crustal thickness varies from 40–45 km thick beneath the western Ethiopian plateau, decreasing to 20–26 km thick in central Afar, and becoming as thin as 16 km in the Danakil Depression (Berckhemer et al., 1975; Makris & Ginzburg, 1987; Mackenzie et al., 2005; Dugda et al., 2005; Stuart et al., 2006; Maguire et al., 2006; Cornwell et al., 2010; Hammond, Kendall, et al., 2011; Reed et al., 2014; Ahmed et al., 2022). The V_P/V_S ratio also shows spatial variation, from 1.7–1.9 beneath the plateau to > 2.0 near magmatic segments where the crustal thickness < 26 km; the high values of V_P/V_S are interpreted as the result of aligned melt stored in interconnected stacked sills in the lower crust (Hammond, 2014).

It is widely accepted that a large low shear velocity province exists beneath the African plate. This long-lived thermo-chemical anomaly has provided the impetus necessary to incite rifting processes in the region, as well as inducing mantle flow that dynamically

supports the excess elevation of Africa (Lithgow-Bertelloni & Silver, 1998; Kendall & Lithgow-Bertelloni, 2016). However, the exact form of mantle upwelling from the core-mantle boundary to the surface is still a matter of debate, particularly in northeast Africa (e.g., Civiero et al., 2015). Hence the regional effect on Eritrea from a sub-crustal velocity anomaly merits investigation. The primary controls on topographic elevation are the isostatic effects of variations in crustal thickness and density; however, the density structure of the mantle, particularly that of a hot thermal anomaly, can affect the pattern of topography observed at the surface (e.g., Bird, 1978; Hager & Richards, 1989; Stephenson et al., 2021). By examining the relationship between topographic elevation and crustal structure in our region and comparing it to the global relationship between these parameters, we can deduce information about mantle structure in Eritrea. Of particular interest is the extent to which intrusive magmatism has affected crustal density, as well as the extent of sub-crustal support from a thermal anomaly.

In this paper, we use a new dataset from a temporary regional seismic deployment across Eritrea to calculate teleseismic receiver functions. Using the H-κ method developed by Zhu and Kanamori (2000) and modified by Ogden et al. (2019), we find the crustal thickness (H) and bulk V_P/V_S ratio (κ) at each station. We supplement our analysis with data from the Afar region, both to update previous work by Hammond, Kendall, et al. (2011), Reed et al. (2014) and Ahmed et al. (2022), and to validate the method of Ogden et al. (2019). We investigate the relationship between elevation and crustal thickness in order to understand the dominant control on topography within the region.

2 Data and Methodology

2.1 Seismic Network

The seismic data used to calculate receiver functions in Eritrea were recorded on a temporary regional seismic network deployed across the country over a period of 16 months (green inverted triangles in Figure 1 (Hammond, Goitom, et al., 2011a)). Six broadband seismic systems were provided by SEIS-UK (five CMGESP and one CMG3T). We supplement seismic data from this regional network with data collected by a temporary local seismic network deployed in the aftermath of Nabro volcano's 2011 eruption (plotted collectively as station NAB in Figure 1 (Hammond, Goitom, et al., 2011b)). Eight 3-component broadband 30 s Güralp seismometers (five CMG-6TD and three CMG-40TD) were provided by SEIS-UK to monitor Nabro's post-eruptive state. The network was fully operational from 31 August 2011 until October 2012. The data were all initially recorded at 100 Hz sample frequency and then switched to 50 Hz sample frequency early in October 2011. To calculate receiver functions in the Afar region of northern Ethiopia we use stations from the AFAR0911 deployment, which ran from 2009 until 2013 (yellow inverted triangles in Figure 1 (Keir & Hammond, 2009)). These stations are 3-component broadband 60 s CMG-ESP Güralp seismometers, recording at 50 Hz sample frequency. Due to the lack of cultural noise, all the data exhibit a generally high signal-to-noise ratio, with excellent data quality (Hammond et al., 2014).

2.2 Teleseismic Dataset

We search the IRIS earthquake catalogue for seismic events with magnitude $M_b \geq 5$, occurring at an epicentral distance greater than 30°. Events are then sorted into two epicentral distance ranges, 30° – 90° and > 60°. The former range is standard for calculating P-to-S receiver functions, as it eliminates the effects of core phases and upper mantle triplications. To increase our azimuthal coverage, we also calculate PP-to-S receiver functions from events in the distance range > 60°.

The data are filtered using a Butterworth bandpass filter with corner frequencies 0.04 and 3 Hz. Seismograms are inspected manually to remove poor quality traces, and

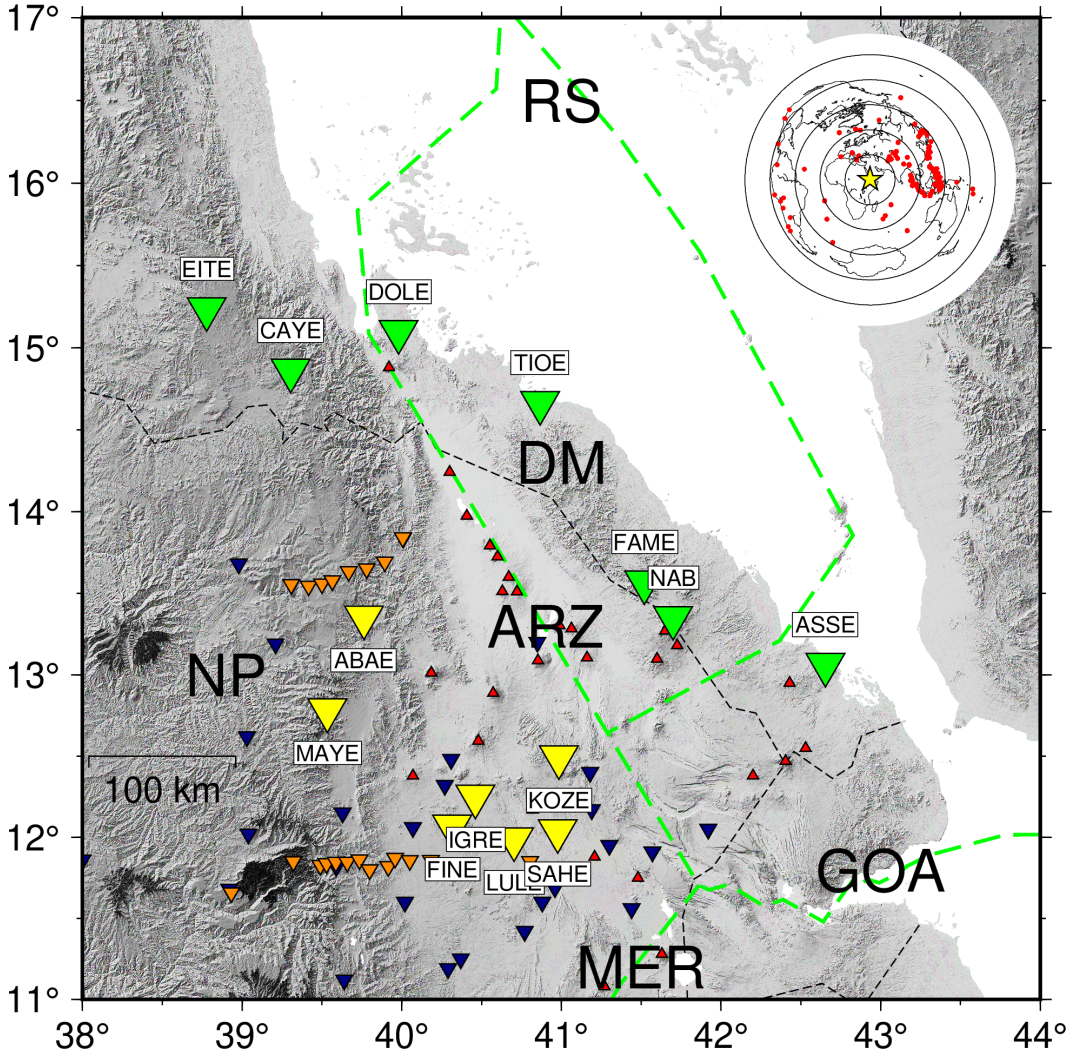

Figure 1. Topographic map of the study region. The boundaries of the Danakil microplate and other plate boundaries are outlined by a dashed green line (Viltres et al., 2020). Dashed black lines demarcate national borders. Seismic stations used in this study are plotted as inverted green and yellow triangles and labelled. Seismic stations from previous studies are plotted as inverted blue triangles (Hammond, Kendall, et al., 2011) and inverted orange triangles (Ahmed et al., 2022). Volcanoes from the Smithsonian Institution Global Volcanism Program are plotted as red triangles (Smithsonian, 2023). Inset shows the locations of the teleseismic earthquakes used in this study, with a yellow star marking the study area. RS: Red Sea, DM: Danakil Microplate, ARZ: Afar Rift Zone, GOA: Gulf of Aden, MER: Main Ethiopian Rift, NP: Nubian Plate.

then analysed based on the signal-to-noise ratio. Source-receiver pairs are kept for further analysis if the P-wave signal-to-noise ratio is >3. This process results in the selection of 102 earthquakes for receiver function construction and processing (inset in Figure 1).

2.3 Methods

2.3.1 Receiver Function Calculation

Receiver function analysis is a well-established technique for investigating velocity contrasts in the crust and upper mantle beneath three-component seismic stations (Langston, 1979). When a compressional P-wave impinges on a velocity contrast, part of the energy is converted into a shear S-wave. These P-to-S conversions are preferentially recorded on the radial components of a seismogram, whilst direct P-wave arrivals are recorded on the vertical component. For teleseismic waves, the incidence angle of the incoming wave will be close to vertical (27° or lower), meaning that we can use the vertical component of motion as a good approximation of the event source. Deconvolution of the vertical component from the radial components removes information common to both (the instrument response, path and source effects). This isolates the response from the local crustal structure along the incoming, near-vertical raypath from a teleseismic earthquake. The resulting receiver functions contain phase arrivals that represent the P-to-S conversion and subsequent reverberations within a layer (the positive polarity PpPs phase, and the negative polarity co-arriving PpSs + PsPs phases, see Figure 3 in Jenkins et al. (2020)). The amplitudes of the arrivals depend on the P-wave incidence angle (ray parameter), the size of the velocity contrast, and whether the wave passes from from a high velocity layer to lower velocity layer, or vice versa. The arrival times of the converted phase and reverberations depend on the depth of the velocity contrast, the P-wave and S-wave velocity between the contrast and the surface, and the ray parameter.

We calculate receiver functions using the iterative time-domain deconvolution method of (Ligorría & Ammon, 1999). This technique iteratively builds receiver functions in the time domain from Gaussian pulses of a set width. For our analysis, we use a range of Gaussian width factors at 0.2 intervals from 0.8–4.0 to produce a set of 17 individual receiver functions for each source-receiver pair. Since periods less than the Gaussian width are not resolvable, our calculated receiver functions have corresponding low-pass filters between 0.4–2.0 Hz. The radial receiver function is then convolved with the vertical component and cross-correlated with the original radial component to evaluate the iterative deconvolution variance (IDVAR). If this variance is $\leq 80\%$, the receiver function is rejected. We also undertake a final manual inspection of the receiver function traces, removing poor quality traces (e.g., ones where the maximum peak arrival is not the direct P-wave arrival, ones with anomalous long wavelength features, and ones which are significantly different from others that sample the same region). This results in a range of 9 to 63 receiver functions per station (Table 1).

2.3.2 H-κ Stacking

We use the H-κ stacking procedure of Zhu and Kanamori (2000) to estimate bulk crustal properties beneath each seismic station (see Supplementary Information Text S1 for further details on the technique). This method has produced accurate estimates of these properties in regions where the crustal structure is simple (e.g., Thompson et al., 2010). However, Eritrea and northern Ethiopia are tectonically complex regions, and we therefore anticipate some potential difficulties in receiver function calculation and interpretation.

The presence of thick sedimentary layers in the study area has been well-established. The Danakil depression hosts a sedimentary basin likely containing up to ∼3–5 km of

Pliocene-Pleistocene-Recent evaporites (Hutchinson & Engels, 1972; Bastow & Keir, 2011; Bastow et al., 2018). Extensional basins in southern and central Afar are filled with Pliocene-Holocene lacustrine, allluvial and volcaniclastic sediments, exceeding 200 m in places (e.g., Renne et al., 1999). Shallow sedimentary layers produce significant P-to-S converted energy that can mask the signal from the Moho and its crustal reverberations, increase the time delay of the direct P-arrival, and enhance the 'ringing' nature of the receiver function signal (e.g., Zelt & Ellis, 1999; Reed et al., 2014; Ogden et al., 2019).

Due to the complicated tectonic history of Afar and Eritrea, we expect significant local differences in the amount of extension and/or thickening due to underplating and intrusion. This can be seen in the variability in previous Moho depth estimates across Afar (e.g., Dugda et al., 2005; Hammond, Kendall, et al., 2011; Lavayssière et al., 2018). It is distinctly observable at single stations with backazimuthal variation in Moho depth, due to the receiver functions from different directions sampling crust of different thickness on either side of the station (e.g., Dugda et al., 2005; Hammond, Kendall, et al., 2011). This is particularly pronounced for stations in Afar that are close to the large border faults, such as ABAE (Hammond, Kendall, et al., 2011). Regions of lower crustal intrusions show a gradational transition between the crust and mantle, as observed by Lavayssière et al. (2018) in Ethiopia. A gradational Moho lowers the amplitude of the Moho P-to-S conversions (Gallacher & Bastow, 2012). The frequency content of the receiver functions thus acquires greater significance for these low amplitude P-to-S conversions, as H-κ stacking will only be sensitive to the Moho using lower frequency receiver functions if the Moho is a more gradational boundary (e.g., Ogden et al., 2019).

For H-κ stacking, V_P is held constant for the whole crust and has to be known *a priori* or assumed. Previous receiver function studies in Afar use a wide range of values for average crustal P-wave velocity (V_P), from 4.65 – 6.5 kms^{-1}, based on criteria such as wide-angle seismic reflection studies or by examining the theoretical relationship between partial melt fraction and seismic velocities. Some allow for variability in V_P between stations (e.g., Reed et al., 2014), whilst others assume one or two values for all stations in their study ((e.g., Dugda et al., 2005; Hammond, Kendall, et al., 2011)).

We therefore employ the cluster analysis approach of Ogden et al. (2019). This rigorously explores the H-κ parameter space, including frequency content of the receiver functions and assumed average crustal V_P, to account for sensitivity of the method to complex crustal structure. The quality control criteria applied to the receiver functions and the cluster analysis provides quantitative evidence for the reliability of H-κ stacking at a station. The number of quality control criteria failed by a station gives an indication of why H-κ stacking has produced an unsatisfactory result. In regions where the Moho is gradational, the ability to adjust the frequency content of the receiver functions means that H-κ stacking remains reliable. The final result will successfully identify the centre of the Moho depth range if the Moho layer thickness is in the range of 0 km to 13 km (Ogden et al., 2019). See the Supplementary Information (Text S2) for more detail on the procedure and the associated uncertainty estimates.

3 Results

Seven stations in Eritrea, including the composite station NAB of the Nabro array stations, and seven stations from the AFAR0911 network produce reliable results using our H-κ stacking procedure (Table 1, Figure 2). Ten quality control criteria assess the quality of these results, described in the Supplementary Information (Text S3 for Eritrea, Text S4 for Afar). Diagnostic result figures for each station are plotted in Figures S1 – S19 in the Supplementary Information. One of the Eritrean stations (EITE) shows strong variation in the Ps arrival time with back-azimuth, a phenomenon previously observed in the region by Dugda et al. (2005) and Hammond, Kendall, et al. (2011). Following these examples, we split the receiver functions at EITE into those arriving from

the east and those arriving from the west, carrying out H-κ stacking on each set separately. These results are plotted as EITE_E and EITE_W, respectively, at the first Moho bounce point of the PpPs multiple for the dominant back azimuth (Figure 2). We follow a similar procedure for the Afar stations ABAE and MAYE, as the receiver functions are almost exclusively from the east for these stations (Figures S11 and S18 in the Supplementary Information). In total, we calculate eight estimates of crustal thickness and V_P/V_S ratio across Eritrea and seven across Afar.

Almost all of the receiver functions show an obvious Ps Moho arrival between 2.5 and 5 s, corresponding to a crustal thickness range of 18.9 – 34.8 km across all stations. This arrival is not always the first positive arrival, which is evidence of a sedimentary layer at the surface. In general, the receiver functions show additional P-to-S arrivals as well as the Moho crustal reverberations, indicating the presence of complex intracrustal structure leading to these subsidiary conversions. The PpPs Moho arrival is observable in most of the receiver functions between 8.5 and 15.5 s, whereas the final arrival of PpSs + PsPs is more ambiguous, occurring between 12 and 20 s. The stations show a range of V_P from 5.9 – 6.5 kms^{-1}, which we determine to be reasonable, given previous controlled source studies (Makris & Ginzburg, 1987; Mackenzie et al., 2005; Maguire et al., 2006).

3.1 Eritrea Stations

Crustal thickness varies across Eritrea. In the Southern Red Sea region, the crust below station ASSE has a thickness of H = 23.5 ± 1.1 km, which is consistent with a previous estimate from the controlled source work of Makris and Ginzburg (1987). Moving onto the Danakil microplate, the crustal thickness beneath Nabro volcano is 25.1 ± 1.1 km. Beneath station FAME it is 20.2 ± 2.2 km and beneath station TIOE it is 18.9 ± 1.0 km. Disrupting the pattern of crustal thinning to the north, station DOLE, positioned close to the Gulf of Zula, has an underlying crustal thickness of 27.2 ± 2.0. In the highlands of Eritrea, the crustal thickness beneath station CAYE is 32.7 ± 1.8 km. The crust under station EITE (W) has a thickness of 34.8 ± 1.5, whereas EITE (E) samples thinner crust, 25.5 ± 1.4 km.

Bulk crustal V_P/V_S ratio also shows variation throughout the country. In the highlands, CAYE has $\kappa = 1.839 \pm 0.030$ and EITE (W) has $\kappa = 1.795 \pm 0.033$, while EITE (E) shows the highest κ estimate of 2.054 ± 0.034. On the Danakil microplate, DOLE has the lowest κ estimate of 1.704 ± 0.033, and TIOE has a higher κ of 2.042 ± 0.036. Moving south, FAME has $\kappa = 1.836 \pm 0.084$, NAB has $\kappa = 1.773 \pm 0.027$ and ASSE has $\kappa = 1.832 \pm 0.027$.

3.2 Afar Stations

On the western plateau of Afar, station ABAE has a crustal thickness of 18.9 ± 0.7 km and station MAYE has a crustal thickness of 20.7 ± 2.4 km. Moving into the rift valley, crustal thicknesses increase, with estimates of 22.5 ± 1.9 km at station FINE, 25.0 ± 2.1 km at station IGRE, 28.3 ± 1.3 km at station KOZE, 25.7 ± 3.9 km at station LULE and 22.2 ± 1.0 km at station SAHE. Within error, these thicknesses are consistent with previous estimates by Hammond, Kendall, et al. (2011), who carried out H-κ stacking at all these stations.

The V_P/V_S ratios calculated at the stations on the western plateau are higher than crustal averages: 2.097 ± 0.023 (ABAE) and 1.911 ± 0025 (MAYE). High V_P/V_S is also seen at stations LULE ($\kappa = 2.041 \pm 0.054$), SAHE ($\kappa = 1.989 \pm 0.022$), FINE ($\kappa = 1.951 \pm 0.025$). IGRE and KOZE show lower V_P/V_S: $\kappa = 1.752 \pm 0.053$ and $\kappa = 1.805 \pm 0.043$, respectively. These are generally consistent with the values found by Hammond, Kendall, et al. (2011), although they tend to estimate a slightly higher V_P/V_S than our

Table 1. H-κ Results

Station	**Long. (°N)**	**Lat. (°E)**	**Elev. (km)**	**H (km)**	**Error (km)**	κ	**Error**	V_P(**kms**$^{-1}$)	**RFs**
				Eritrea Stations					
ASSE	13.06	42.65	0.019	24	1	1.83	0.03	5.9	14
CAYE	14.86	39.31	2.435	33	2	1.84	0.03	6.1	28
EITE (W)	15.24	38.28	2.171	35	2	1.80	0.03	6.2	9
EITE (E)	15.24	39.12	1.471	26	1	2.05	0.03	6.2	36
DOLE	15.10	39.98	0.088	27	2	1.70	0.03	6.5	9
FAME	13.57	41.52	0.622	20	2	1.84	0.08	6.4	26
NAB	13.35	41.7	1.272	25	1	1.77	0.03	5.9	63
TIOE	14.67	40.87	0.043	19	1	2.04	0.04	6.0	20
				Afar Stations					
ABAE	13.35	39.76	1.447	19	1	2.10	0.02	6.2	53
FINE	12.07	40.32	0.782	23	2	1.95	0.03	6.3	23
IGRE	12.25	40.46	0.675	25	2	1.75	0.05	5.9	42
KOZE	12.49	40.98	0.543	28	1	1.81	0.04	5.9	34
LULE	11.99	40.70	0.594	26	4	2.04	0.05	6.5	20
MAYE	12.78	39.53	2.440	21	2	1.91	0.023	6.5	26
SAHE	12.04	40.98	0.365	22	1	1.99	0.02	5.9	23

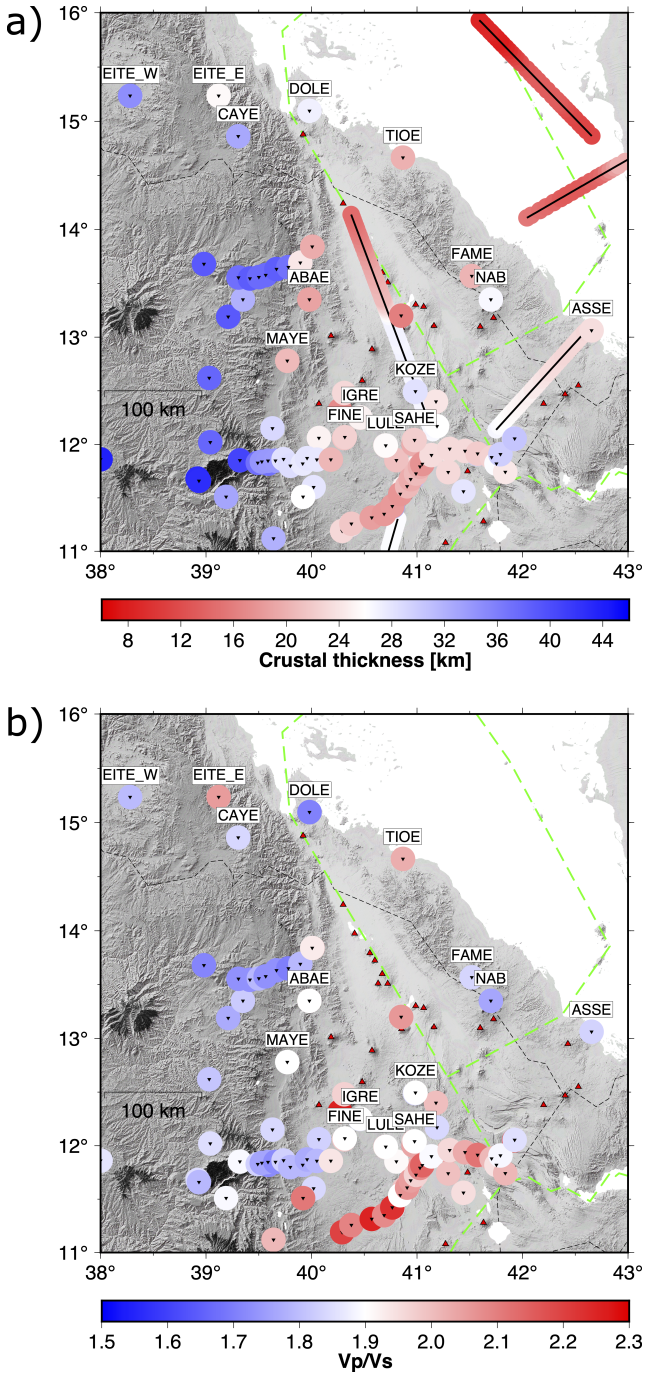

Figure 2. Regional map showing the results of this study alongside previous estimates of crustal thickness and V_P/V_S ratio (see Table S1 in the Supplementary Information for a full list). The seismic stations are plotted as inverted triangles, with those used in this study labelled. The boundaries of the Danakil microplate and other plate boundaries are outlined by a dashed green line (Viltres et al., 2020). Dashed black lines demarcate national borders. Volcanoes from the Smithsonian Institution Global Volcanism Program are plotted as red triangles (Smithsonian, 2023). a) The crustal thickness estimates. Thick black lines mark the profiles for controlled source work by Berckhemer et al. (1975); Makris and Ginzburg (1987); Egloff et al. (1991); Mackenzie et al. (2005); Maguire et al. (2006). Other estimates of crustal thickness come from Hammond, Kendall, et al. (2011), Reed et al. (2014) and Ahmed et al. (2022). b) V_P/V_S ratio estimates from this study and from Hammond, Kendall, et al. (2011), Reed et al. (2014) and Ahmed et al. (2022).

results. This consistency gives confidence to the H-κ stacking procedure we employ, as well as our selected values of V_P.

4 Discussion

4.1 Implications for rifting through the Gulf of Zula

In contrast to the diffuse extensional province of the Afar Depression, where rifting shows clear signs of jumping location as the triple junction migrated northward (Hammond, Kendall, et al., 2011), the rift axis through the Gulf of Zula is more focussed. Station DOLE, despite its proximity to the gulf, has a relatively thick crust of 27.2 km. Admittedly, the receiver functions mainly sample the crust to the north-east of the station (and thus further from the rift), due to the back-azimuthal coverage. Still, in comparison to Afar, where rifting occurs over distances of ∼175 km (Kogan et al., 2012), our crustal thickness estimate for DOLE indicates a more focused extension. Viltres et al. (2020) conclude from their GPS study that inter-rifting deformation is not localised directly in the gulf. Instead it is accommodated by volcanic vents and distributed faults to the west. Station EITE (E) is almost due west of DOLE and has a thinner crust of 25.5 km, which is perhaps an indication of an overall westward shift in active deformation (Viltres et al., 2020).

When rifting initiates on oceanic crust close to a continental margin, the active spreading ridge can propagate onto continental crust and continue rifting, creating a new ridge within continental crust (Müller et al., 2001). Eventually a small segment of stretched crust is severed away from the continent, leading to isolated microcontinents such as the Jan Mayen microcontinent, the Seychelles, the East Tasman Plateau and the Gilbert Seamount Complex in the Tasman Sea. We propose that a similar process is currently initiating through the Gulf of Zula, where the Red Sea Rift has jumped onto the continental margin due to the rheological weakness of the crust. If rifting in Afar progresses to seafloor spreading, the Danakil microplate could become separated from the rest of the continent by an oceanic basin.

4.2 The nature of the Danakil microplate

Our crustal thickness estimates for the stations located on the Danakil block are lower than the global average value for extended continental crust of 30.5 km (Christensen & Mooney, 1995). They are also 10–15 km thinner than estimates for stations found on the plateaus (Figure 2). Indeed, stations TIOE and FAME show thicknesses that are similar to those found in the rift valley of Afar. While we lack constraints from the interior of the Danakil highlands, we nevertheless propose that the Danakil is not 'relatively unstretched' as has been previously claimed (Wolfenden et al., 2005), but has undergone a significant amount of deformation and crustal thinning. Two-dimensional area balancing in a previous plate kinematic reconstruction study confirms this conclusion, suggesting that the Danakil block has undergone a minimum of 200% stretch since the onset of rifting (Figure 3, Redfield et al., 2003).

4.3 Melt in the crust in Eritrea

Station EITE (E) has a V_P/V_S ratio of 2.054, which is significantly higher than the average value for continental crust of 1.768 (Christensen, 1996). V_P/V_S ratios above 1.9 cannot be accounted for by differences in rock composition (Thompson et al., 2010). Instead, these elevated values are typically explained by the presence of fluid in the crust, which decreases the S-wave velocity without significantly affecting the P-wave velocity (e.g., Watanabe, 1993). EITE (E) is located on the edge of the plateau, close to the Gulf of Zula. It shows strong similarity to stations MAYE and ABAE, which are positioned on the rift shoulder in northern Afar and also show high V_P/V_S ratios. We therefore pro-

pose that partial melt in the crust is present along the edge of the western plateau from northern Afar all the way up to Eritrea. Another very elevated V_P/V_S value of 2.042 is observed at station TIOE. In general, crustal thickness in the region is negatively correlated with the bulk V_P/V_S ratio (see Figure S20 in the Supplementary Information), implying that the thinnest crust is also the most intruded. This indicates that the stretched, thinned nature of the Danakil microplate crust has facilitated the presence of partial melt. Thus, it is likely that magmatic extension continues to play a dominant role in the final stages of continental breakup in Eritrea. Stations ASSE, CAYE and FAME have V_P/V_S values that are greater than 1.8, which are closer to the expected values for oceanic crust (Christensen, 1996). The most likely explanation for this is the presence of magmatic intrusions causing the continental crust to have a more mafic tendency.

Our V_P/V_S result at Nabro volcano (station NAB, Figure 2) is relatively low (1.773). Nabro erupted in 2011 and therefore the crust beneath the volcano might be expected to have an elevated V_P/V_S ratio, reflecting melt storage. However, Hammond (2014) demonstrated that the relative orientation and alignment of melt has a significant effect on H-κ estimates. If melt is vertically aligned, the shear wave conversion will be split as it passes through, with each of the split waves producing different κ estimates due to their different velocities. When there is good back-azimuthal coverage at a station, the overall stacking procedure will be dominated by the slow shear wave velocity, and thus produces a higher V_P/V_S estimate. This effect becomes less pronounced as melt becomes more horizontally aligned. We therefore propose that Nabro could host melt in stacked horizontal sills in the crust, which is why the V_P/V_S ratio estimate produced by H-κ stacking is not particularly high. This conclusion is supported by the petrological analysis of Donovan et al. (2018), who concluded that Nabro hosts distinct batches of magma in sills throughout the crust. Alternatively, the overall crust at Nabro could be melt-depleted, with melt travelling directly up from the mantle to shallow storage regions just prior to eruption. Nabro's high crustal thickness could be due to magmatic intrusions and additions occurring through time. Again, there is petrological evidence for a significant amount of old eruptive products in the crust beneath Nabro, due to the presence of xenocrystic material in the erupted magmas Donovan et al. (2018). Unfortunately, the back-azimuthal coverage is not comprehensive enough to carry out a crustal anisotropy study at Nabro to investigate these proposals further (e.g., Liu & Niu, 2012).

4.4 Topographic elevation and crustal structure

Topographic elevation can primarily be attributed to the isostatic effects of crustal thickness and density variations in the crust (e.g., Anderson & Anderson, 2010). However, a secondary control on continental topography is the density structure of the mantle (e.g., Lithgow-Bertelloni & Silver, 1998; Hoggard et al., 2021; Stephenson et al., 2021). Our results can therefore place indirect constraints on crustal and mantle density structure. We investigate the relationship between topographic elevation (ϵ) and crustal thickness for the Eritrea and Afar region (Figure 3a).

There is a demonstrable linear relationship between H and ϵ, suggesting that 3 km variation in the topographic elevation in the study area can be ascribed to variation in crustal thickness. A similar relationship between topographic elevation and crustal thickness is widely known for a global dataset (Figure 5 in Stephenson et al., in review; Lamb et al., 2020) and plotted in Figure 3a) for comparison. However, our regional study shows two key differences which provide a rare opportunity to quantify the regional properties of the crust and uppermost mantle. First, the slope is lower, indicating that there is a different average crustal and/or mantle density to global average values. This difference is not unexpected given the rift setting of the region, although it has seldom been quantified (e.g., Ebinger et al., 1989; Tiberi et al., 2003). Furthermore, the intercept crustal thickness value is shifted upwards, which implies significant levels of sub-plate topographic support which must arise from processes operating in the mantle beneath the region. In

other words, topographic elevation is generally higher than would be expected for a given value of crustal thickness if crustal isostasy were the only control on topography (Airy, 1855; Pratt, 1855). Here, we use these observations to provide new constraints on lithospheric and sub-plate density structure.

4.4.1 Crustal density estimate

We can quantify the difference in crustal density in our study region to the global average by using the gradient of the plot in Figure 3a) to estimate a crustal density for Eritrea and Afar (e.g., Lamb et al., 2020; Stephenson et al., in review). The relationship between crustal thickness, H and topographic elevation, ϵ, depends on the ratio $(\rho_a - \rho_c)/\rho_a$, where ρ_c is crustal density and ρ_a is asthenospheric mantle density. This relationship assumes Airy isostatic equilibrium and that topography is compensated in the asthenospheric mantle.

First, we approximate a value for ρ_a, by calculating the effects of temperature and pressure upon mantle rocks. Mantle density as a function of pressure, P, and T, is given by

$$\rho(P,T) \approx \rho_{m_\circ} \exp\left(\frac{P}{K} - \alpha T\right), \tag{1}$$

where the thermal expansivity coefficient $\alpha = 3.28 \times 10^{-5}$ K^{-1}, $K = 140$ GPa is the bulk modulus of the mantle and $\rho_{m_\circ} = 3330$ kg m^{-3} is mantle density at surface pressure and temperature. Ball et al. (2021) estimate that the sub-plate temperature beneath north-eastern Ethiopia is ∼1465 °C and the lithospheric thickness, z_l, is ∼ 35 km. However, since our crustal thickness estimates suggest that the crust in Eritrea and Afar can reach up to 45 km thick, we use this higher value for the depth to the base of the lithosphere, noting that this may be an upper bound. We use the relationship $P_l = \overline{\rho} g z_l$ to find the pressure at the base of the lithosphere, where $\overline{\rho} \approx 3000$ kg m^{-3} is overburden density, z is depth and $g = 9.81$ m s^{-2} is acceleration due to gravity. We find that $P \approx 1.3$ GPa. Therefore $\rho_a \approx 3220$ kg m^{-3}.

We apply a non-biased linear regression (i.e., a Deming regression) that assumes uncertainty in both topography and crustal thickness (±30 m and ±3 km, respectively) and find that $(\rho_a - \rho_c)/\rho_a = 0.086$, which is indeed substantially lower than the global average value of around 0.11–0.13 (Figure 3; Lamb et al., 2020; Stephenson et al., in review). Using our estimated value of ρ_a, we find that in Eritrea and Afar, $\rho_c \approx 2940$ kg m^{-3}. As expected, this value is higher than the global average value of $\rho_c \approx 2880$ kg m^{-3}. The elevated crustal density likely reflects the substantial magmatic intrusions and additions to the crust by mafic volcanic rocks that have taken place in this region. It furthermore provides a new and independent constraint that adds weight to our earlier conclusion that the high V_P/V_S ratios we observe are likely to be due to magmatic activity.

4.5 Sub-crustal support

It is well-established that mantle upwelling and flow from a large low shear velocity province have had a significant effect on the tectonics and topography of Africa. While the magnitude of sub-crustal support from the mantle has been estimated in Ethiopia, a paucity of data means that the extent of the hot mantle swell northwards into Eritrea has not been well-constrained. From the relationship between crustal thickness and elevation, it is clear that Eritrean topography is anomalously high given the crustal thickness. It is notable that, for $H \approx$ 10-20 km, the topography is approximately at sea level. However, globally, the average crustal thickness is about 32.8 km for regions at sea level (Lamb et al., 2020; Stephenson et al., in review). To illustrate this point, take station CAYE, which has crustal thickness of $H = 32.7$ km, which is almost exactly the thickness of crust that is globally expected to reside at sea level. Instead, CAYE is located

at an elevation of about $\epsilon = 2.1$ km. This marked offset implies a significant level of regional sub-crustal support that sustains the topography in Eritrea and Afar that we can, for the first time, quantify regionally across Eritrea.

A hot mantle plume can generate uplift in three interconnected ways (e.g., Forte et al., 1993; Hoggard et al., 2021). First, the upward flow of the plume produces viscous forces that cause vertical tractions on the base of the plate. Second, the buoyancy of the hot mantle material generates isostatic uplift at the surface. Finally, erosion of the base of the lithosphere by heat and/or melt and fluid infiltration can thin the lithospheric mantle. Here, we explore the effects of the second and third processes on Eritrea and Afar by estimating the uplift that is generated both by a hot thermal anomaly beneath the plate and by thinning of the lithospheric mantle in the region.

Uplift above a hot asthenospheric anomaly of thickness h and excess temperature ΔT is given by

$$U = \frac{\alpha T_1}{1 - \alpha T_1} \left(\frac{a_1^2}{2a_0} + \frac{a_0}{2} - a_1 + \frac{\Delta T}{T_1} h \right), \tag{2}$$

where the thermal expansivity $\alpha = 3.28{\times}10^{-5}$ K^{-1}, a_0 and a_1 are initial and final lithospheric thicknesses and T_1 is ambient mantle temperature. We assume an initial lithospheric thickness of 150 km, and take an asthenospheric channel to be $h = 150$ km thick (McKenzie, 1978). We constrain ΔT and a_1 using the method of Hoggard et al. (2021) and Richards et al. (2020) to calculate mantle temperatures from upper mantle shear wave velocities. Hoggard et al. (2021) applied the approach to the tomographic model of Celli et al. (2020); see their paper for further detail. Contouring the 1175 °C isotherm within these temperature models yields estimates of present day lithospheric thickness, a_1. From this model, we extract ΔT. We also extract a_1, the depth to the base of the lithosphere. Using Equation 2, we calculate an uplift estimate of 1.4–2.2 km; the amount of topography that is likely to be supported by sub-crustal mantle structure. This range is consistent with the 2.2 km of sub-crustal support implied by the temperature and lithospheric thickness estimate obtained by Ball et al. (2021).

From Figure 3a), the level of regional sub-crustal support can also, independently be estimated by using the offset in intercept values between the regional isostatic relationship and the global one. We find that $\Delta\epsilon = 2.2 \pm 0.4$ km (plotted as the shaded region on Figure 3b). This range overlaps with our previous estimates of uplift above a hot thermal anomaly and thin lithosphere. These results are consistent with a major mantle plume residing beneath Afar and Eritrea. To summarise, we have shown by using three independent sets of observations, that topography beneath Eritrea is likely to be supported to a significant extent by sub-crustal processes including thinner than average lithospheric mantle and sub-plate temperature anomalies. Our simple calculations clearly illustrate the spatial extent of this swell, which is not isolated to the Ethiopian Highlands, but instead extends regionally, beneath both regions of thin and thick crust.

It is important to note that our results do not attempt to estimate the mantle flow component of sub-crustally supported topography, nor do they attempt to quantify the component arising from below the uppermost 200 km of the mantle. Furthermore, a potentially significant component of topographic support from the lithospheric mantle arises from lithospheric extension. However, the Ethiopian swell is clearly a widespread feature that extends into Eritrea and sub-plate temperature anomalies appear to be required to explain the height of Eritrean topography.

4.6 Future work

We observe variation in bulk crustal properties across Eritrea. Our temporary seismic network is distributed across the country, with significant distances between stations. In particular, we note that we were unable to deploy a station within the Danakil Alps, and that a station on Alid volcano was only operational for three months. Future de-

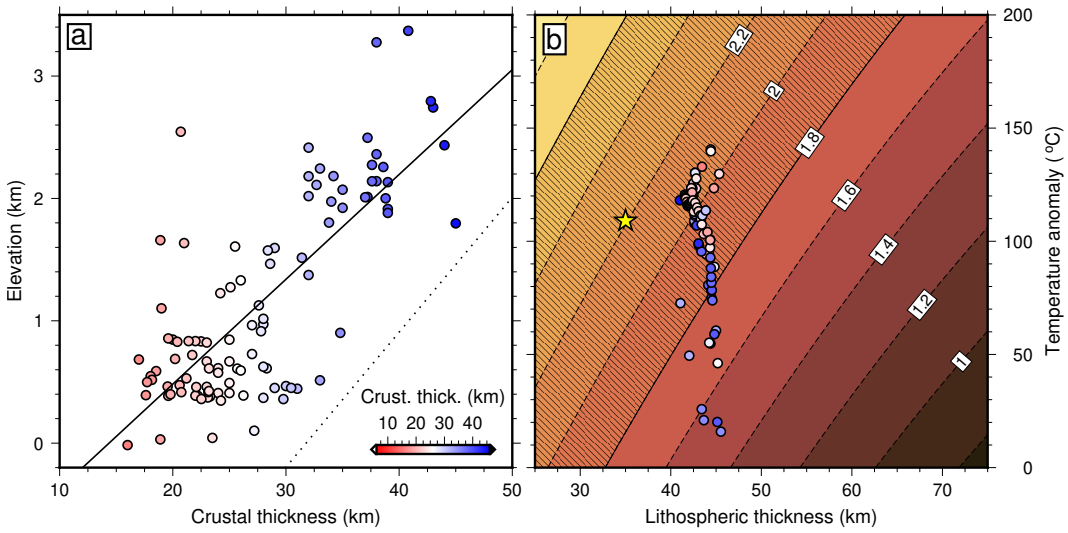

Figure 3. Crustal and mantle structure. (a) Topographic elevation plotted against crustal thickness estimates (coloured circles) for the study region, from this study and the previous receiver function studies of Hammond, Kendall, et al. (2011); Reed et al. (2014); Ahmed et al. (2022). Elevation estimates are from the GMT Global Earth Relief grid, with the topography low-pass filtered for wavelengths > 30km (Wessel et al., 2019). The black line is the best-fitting regional isostatic relationship where $(\rho_a - \rho_c)/\rho_a = 0.086$; the dotted black line is the average global isostatic relationship where $(\rho_- \rho_c)/\rho_a = 0.110$ (Stephenson et al., in review). (b) Sub-crustally supported topography as a function of asthenospheric mantle temperature and lithospheric thickness, assuming a temperature anomaly is constrained to a 150 km thick channel and equilibrium lithospheric thickness is 150 km. Contours indicate elevation, ϵ. The shaded area represents the range of regional sub-crustal support ($\Delta\epsilon = 2.2 \pm 0.4$ km) estimated from the offset in intercept values between the regional crustal thickness-elevation relationship and the global one. The plotted circles are tomographically estimated asthenospheric temperatures as a function of lithospheric thickness beneath seismic stations and are coloured by crustal thickness. The yellow star is plotted at the sub-plate temperature and lithospheric thickness given by inverse modelling of rare earth element compositions (Ball et al., 2021).

ployments will hopefully address these data gaps—we propose that attention should be given to the Gulf of Zula, the Danakil Alps, and the region between Nabro volcano and the Eritrea-Djibouti border.

5 Conclusion

We have produced the first estimates of crustal thickness and bulk crustal V_P/V_S ratio in Eritrea. We calculate receiver functions from a temporary regional seismic array and apply the modified H-κ stacking technique of Ogden et al. (2019) to constrain the bulk crustal properties at eight locations. To validate this procedure, we also carry out H-κ stacking at stations in Afar, producing estimates that are consistent with previous studies in the region.

This study has revealed the heterogeneity of Eritrean crust. We calculate a variability in crustal thickness of ∼16 km throughout the study area, ranging from ∼19 km — ∼35 km. This reveals that the Danakil microplate is not an undeformed, unified block, but rather has experienced extension and crustal thinning resulting in crust as thin as 18.9 km. We find that the propagation of the Red Sea Rift into Afar is localised within the Gulf of Zula, with thicker crust (25.5 km) found directly to the east of the gulf. We also see variation in V_P/V_S ratio across Eritrea. Some stations have values typical of continental crust ∼1.77. Others show higher values of 1.8–1.86, likely a consequence of alteration by magmatic intrusion or addition to the crust. Two stations have V_P/V_S greater than 2.0, which we associate with the presence of partial melt, suggesting that magmatic extension continues to be important in the final stages of continental rifting.

By examining the relationship between topographic elevation and crustal thickness, we observe a deviation from the global relationship between these parameters. We estimate a denser crust across Eritrea and Afar ($\rho_c \approx 2940$ km m^{-3}), which is evidence for intrusive magmatism altering the composition of the crust to be more mafic. Our results reveal that the height of the topography is anomalously high for the observed thicknesses of Eritrean crust, implying a level of sub-crustal support from a hot thermal anomaly beneath the crust.

Our observations of crustal properties address the previously existing data gap in Eritrea, provide a useful base for further investigations of the Eritrean crust and mantle, and give insights into the processes responsible for topographic elevation in the region.

Open Research

The seismic data used in this study are from the Eritrea Seismic Project (Hammond, Goitom, et al., 2011a), the Nabro Urgency Array (Hammond, Goitom, et al., 2011b), and the AFAR0911 network (Keir & Hammond, 2009), all publicly available through IRIS Data Services (http://service.iris.edu/fdsnws/dataselect/1/). When analysing the seismograms, we made use of the Seismic Analysis Code software (Helffrich et al., 2013) and the iterative deconvolution code "iterdecon", available online at http://eqseis.geosc.psu.edu/cammon/HTML/RftnDocs/thecodes01.html. Figures and maps were plotted using Generic Mapping Tools (GMT) version 6 (Wessel et al., 2019) licensed under LGPL version 3 or later, available at https://www.genericmapping-tools.org.

Acknowledgments
The seismic data were collected with funding from the Natural Environment Research Council (NERC) projects NE/J012297/1, NE/E007414/1, and NE/D008611/1 and NSF grant EAR-0635789. The UK seismic instruments and data management facilities were provided under loan number 976 by SEIS-UK at the University of Leicester. The facil-

ities of SEIS-UK are supported by NERC under Agreement R8/H10/64. Author MG was supported by a Doctoral Training Partnership studentship from NERC [NE/S007474/1]. We gratefully acknowledge the cooperation we received from the Eritrea Institute of Technology, Eritrean government, Southern and Northern Red Sea Administrations, local subzones and village administrations. We thank the Department of Mines, Ministry of Energy and Mines for their continued support throughout the Eritrean project. We also thank Addis Ababa University, the Ethiopian Federal Government, Afar National Regional State Government and Ethioder tour and travel for vital help and support during the Afar deployment. Special thanks go to Zerai Berhe, Mebrahtu Fisseha, Michael Eyob, Ahmed Mohammed, Kibrom Nerayo, Asresehey Ogbatsien, Andemichael Solomon and Isaac Tuum. We thank Alem Kibreab for vital help in facilitating the fieldwork. IRIS Data Services are funded through the Seismological Facilities for the Advancement of Geoscience (SAGE) Award of the National Science Foundation under Cooperative Support Agreement EAR-1851048.

References

Ahmed, A., Doubre, C., Leroy, S., Keir, D., Pagli, C., Hammond, J. O., ... others (2022). Across and along-strike crustal structure variations of the western Afar margin and adjacent plateau: Insights from receiver functions analysis. *Journal of African Earth Sciences*, *192*, 104570.

Airy, G. B. (1855). III. On the computation of the effect of the attraction of mountain-masses, as disturbing the apparent astronomical latitude of stations in geodetic surveys. *Philosophical Transactions of the Royal Society of London*(145), 101–104.

Anderson, R. S., & Anderson, S. P. (2010). *Geomorphology: the mechanics and chemistry of landscapes*. Cambridge University Press.

Ball, P., White, N., Maclennan, J., & Stephenson, S. (2021). Global influence of mantle temperature and plate thickness on intraplate volcanism. *Nature communications*, *12*(1), 1–13.

Barberi, F., & Varet, J. (1977). Volcanism of Afar: Small-scale plate tectonics implications. *Geological Society of America Bulletin*, *88*(9), 1251–1266.

Barton, A., & White, R. (1997). Volcanism on the Rockall continental margin. *Journal of the Geological Society*, *154*(3), 531–536.

Bastow, I., Booth, A., Corti, G., Keir, D., Magee, C., Jackson, C. A.-L., ... Lascialfari, M. (2018). The development of late-stage continental breakup: Seismic reflection and borehole evidence from the Danakil Depression, Ethiopia. *Tectonics*, *37*(9), 2848–2862.

Bastow, I., & Keir, D. (2011). The protracted development of the continent–ocean transition in Afar. *Nature Geoscience*, *4*(4), 248–250.

Berckhemer, H., Baier, B., Bartelsen, H., Behle, A., Burkhardt, H., Gebrande, H., ... Vees, R. (1975). Deep seismic soundings in the Afar region and on the highland of Ethiopia. *Afar depression of Ethiopia*, *1*, 89–107.

Bird, P. (1978). Initiation of intracontinental subduction in the Himalaya. *Journal of Geophysical Research: Solid Earth*, *83*(B10), 4975–4987.

Celli, N., Lebedev, S., Schaeffer, A., Ravenna, M., & Gaina, C. (2020). The upper mantle beneath the South Atlantic Ocean, South America and Africa from waveform tomography with massive data sets. *Geophysical Journal International*, *221*(1), 178–204.

Christensen, N. I. (1996). Poisson's ratio and crustal seismology. *Journal of Geophysical Research: Solid Earth*, *101*(B2), 3139–3156.

Christensen, N. I., & Mooney, W. D. (1995). Seismic velocity structure and composition of the continental crust: A global view. *Journal of Geophysical Research: Solid Earth*, *100*(B6), 9761–9788.

Civiero, C., Hammond, J. O., Goes, S., Fishwick, S., Ahmed, A., Ayele, A., ... oth-

ers (2015). Multiple mantle upwellings in the transition zone beneath the northern East-African Rift system from relative P-wave travel-time tomography. *Geochemistry, Geophysics, Geosystems*, *16*(9), 2949–2968.

Cornwell, D., Maguire, P., England, R., & Stuart, G. (2010). Imaging detailed crustal structure and magmatic intrusion across the Ethiopian Rift using a dense linear broadband array. *Geochemistry, Geophysics, Geosystems*, *11*(1).

Donovan, A., Blundy, J., Oppenheimer, C., & Buisman, I. (2018). The 2011 eruption of Nabro volcano, Eritrea: perspectives on magmatic processes from melt inclusions. *Contributions to Mineralogy and Petrology*, *173*(1), 1–23.

Dugda, M. T., Nyblade, A. A., Julia, J., Langston, C. A., Ammon, C. J., & Simiyu, S. (2005). Crustal structure in Ethiopia and Kenya from receiver function analysis: Implications for rift development in eastern Africa. *Journal of Geophysical Research: Solid Earth*, *110*(B1).

Ebinger, C., Bechtel, T., Forsyth, D., & Bowin, C. (1989). Effective elastic plate thickness beneath the East African and Afar plateaus and dynamic compensation of the uplifts. *Journal of Geophysical Research: Solid Earth*, *94*(B3), 2883–2901.

Ebinger, C., & Casey, M. (2001). Continental breakup in magmatic provinces: An Ethiopian example. *Geology*, *29*(6), 527–530.

Egloff, F., Rihm, R., Makris, J., Izzeldin, Y., Bobsien, M., Meier, K., ... Warsi, W. (1991). Contrasting structural styles of the eastern and western margins of the southern Red Sea: the 1988 SONNE experiment. *Tectonophysics*, *198*(2-4), 329–353.

Forte, A. M., Peltier, W. R., Dziewonski, A. M., & Woodward, R. L. (1993). Dynamic surface topography: A new interpretation based upon mantle flow models derived from seismic tomography. *Geophysical Research Letters*, *20*(3), 225–228.

Gallacher, R., & Bastow, I. (2012). The development of magmatism along the Cameroon Volcanic Line: Evidence from teleseismic receiver functions. *Tectonics*, *31*(3).

Hager, B. H., & Richards, M. A. (1989). Long-wavelength variations in Earth's geoid: physical models and dynamical implications. *Philosophical Transactions of the Royal Society of London. Series A, Mathematical and Physical Sciences*, *328*(1599), 309–327.

Hammond, J. (2014). Constraining melt geometries beneath the Afar Depression, Ethiopia from teleseismic receiver functions: The anisotropic H-κ stacking technique. *Geochemistry, Geophysics, Geosystems*, *15*(4), 1316–1332.

Hammond, J., Goitom, B., & Kendall, J.-M. (2014). Rifting in the Horn of Africa: The Eritrea Seismic Project (June 2011–October 2012). *NERC Geophysical Equipment Facility*, *Scientific Report 913*.

Hammond, J., Goitom, B., Kendall, J. M., & Ogubazghi, G. (2011a). *Eritrea Seismic Project.* International Federation of Digital Seismograph Networks. Retrieved from `https://www.fdsn.org/networks/detail/5H_2011/` doi: 10.7914/SN/5H_2011

Hammond, J., Goitom, B., Kendall, J. M., & Ogubazghi, G. (2011b). *Nabro Urgency Array.* International Federation of Digital Seismograph Networks. Retrieved from `https://www.fdsn.org/networks/detail/4H_2011/` doi: 10.7914/SN/4H_2011

Hammond, J., Kendall, J.-M., Stuart, G., Keir, D., Ebinger, C., Ayele, A., & Belachew, M. (2011). The nature of the crust beneath the Afar triple junction: Evidence from receiver functions. *Geochemistry, Geophysics, Geosystems*, *12*(12).

Helffrich, G., Wookey, J., & Bastow, I. (2013). *The seismic analysis code: A primer and user's guide.* Cambridge University Press.

Hoggard, M., Austermann, J., Randel, C., & Stephenson, S. (2021). Observational

estimates of dynamic topography through space and time. *Mantle convection and surface expressions*, 371–411.

Hutchinson, R., & Engels, G. (1972). Tectonic evolution in the southern Red Sea and its possible significance to older rifted continental margins. *Geological Society of America Bulletin*, *83*(10), 2989–3002.

Jenkins, J., Stephenson, S. N., Martínez-Garzón, P., Bohnhoff, M., & Nurlu, M. (2020). Crustal thickness variation across the Sea of Marmara region, NW Turkey: A reflection of modern and ancient tectonic processes. *Tectonics*, *39*(7), e2019TC005986.

Keir, D., Bastow, I., Pagli, C., & Chambers, E. L. (2013). The development of extension and magmatism in the Red Sea rift of Afar. *Tectonophysics*, *607*, 98–114.

Keir, D., & Hammond, J. (2009). *AFAR0911.* International Federation of Digital Seismograph Networks. Retrieved from `https://www.fdsn.org/networks/detail/2H_2009/` doi: 10.7914/SN/2H_2009

Kendall, J.-M., & Lithgow-Bertelloni, C. (2016). Why is Africa rifting? *Special Publications*, *420*(1), 11–30.

Kogan, L., Fisseha, S., Bendick, R., Reilinger, R., McClusky, S., King, R., & Solomon, T. (2012). Lithospheric strength and strain localization in continental extension from observations of the East African Rift. *Journal of Geophysical Research: Solid Earth*, *117*(B3).

Lamb, S., Moore, J. D., Perez-Gussinye, M., & Stern, T. (2020). Global whole lithosphere isostasy: implications for surface elevations, structure, strength, and densities of the continental lithosphere. *Geochemistry, Geophysics, Geosystems*, *21*(10), e2020GC009150.

Langston, C. A. (1979). Structure under Mount Rainier, Washington, inferred from teleseismic body waves. *Journal of Geophysical Research: Solid Earth*, *84*(B9), 4749–4762.

Lavayssière, A., Rychert, C., Harmon, N., Keir, D., Hammond, J. O., Kendall, J.-M., ... Leroy, S. (2018). Imaging lithospheric discontinuities beneath the northern East African Rift using S-to-P receiver functions. *Geochemistry, Geophysics, Geosystems*, *19*(10), 4048–4062.

Ligorría, J. P., & Ammon, C. J. (1999). Iterative deconvolution and receiver-function estimation. *Bulletin of the seismological Society of America*, *89*(5), 1395–1400.

Lithgow-Bertelloni, C., & Silver, P. G. (1998). Dynamic topography, plate driving forces and the African superswell. *Nature*, *395*(6699), 269–272.

Liu, H., & Niu, F. (2012). Estimating crustal seismic anisotropy with a joint analysis of radial and transverse receiver function data. *Geophysical Journal International*, *188*(1), 144–164.

Mackenzie, G., Thybo, H., & Maguire, P. (2005). Crustal velocity structure across the Main Ethiopian Rift: results from two-dimensional wide-angle seismic modelling. *Geophysical Journal International*, *162*(3), 994–1006.

Maguire, P., Keller, G., Klemperer, S., Mackenzie, G., Keranen, K., Harder, S., ... others (2006). Crustal structure of the northern Main Ethiopian Rift from the EAGLE controlled-source survey; a snapshot of incipient lithospheric break-up. *Geological Society, London, Special Publications*, *259*(1), 269–292.

Makris, J., & Ginzburg, A. (1987). The Afar Depression: transition between continental rifting and sea-floor spreading. *Tectonophysics*, *141*(1-3), 199–214.

Manighetti, I., Tapponnier, P., Gillot, P., Jacques, E., Courtillot, V., Armijo, R., ... King, G. (1998). Propagation of rifting along the Arabia-Somalia plate boundary: Into Afar. *Journal of Geophysical Research: Solid Earth*, *103*(B3), 4947–4974.

McKenzie, D. (1978). Some remarks on the development of sedimentary basins. *Earth and Planetary science letters*, *40*(1), 25–32.

Mohr, P. (1989). Nature of the crust under Afar: new igneous, not thinned continental. *Tectonophysics*, *167*(1), 1–11.

Müller, R. D., Gaina, C., Roest, W. R., & Hansen, D. L. (2001). A recipe for microcontinent formation. *Geology*, *29*(3), 203–206.

Ogden, C., Bastow, I. D., Gilligan, A., & Rondenay, S. (2019). A reappraisal of the H–κ stacking technique: implications for global crustal structure. *Geophysical Journal International*, *219*(3), 1491–1513.

Pratt, J. H. (1855). I. On the attraction of the Himalaya Mountains, and of the elevated regions beyond them, upon the plumb-line in India. *Philosophical Transactions of the Royal Society of London*(145), 53–100.

Redfield, T., Wheeler, W., & Often, M. (2003). A kinematic model for the development of the Afar Depression and its paleogeographic implications. *Earth and Planetary Science Letters*, *216*(3), 383–398.

Reed, C. A., Almadani, S., Gao, S. S., Elsheikh, A. A., Cherie, S., Abdelsalam, M. G., ... Liu, K. H. (2014). Receiver function constraints on crustal seismic velocities and partial melting beneath the Red Sea rift and adjacent regions, Afar Depression. *Journal of Geophysical Research: Solid Earth*, *119*(3), 2138–2152.

Renne, P. R., WoldeGabriel, G., Hart, W. K., Heiken, G., & White, T. D. (1999). Chronostratigraphy of the Miocene–Pliocene Sagantole Formation, Middle Awash Valley, Afar rift, Ethiopia. *Geological Society of America Bulletin*, *111*(6), 869–885.

Richards, F. D., Hoggard, M. J., White, N., & Ghelichkhan, S. (2020). Quantifying the relationship between short-wavelength dynamic topography and thermomechanical structure of the upper mantle using calibrated parameterization of anelasticity. *Journal of Geophysical Research: Solid Earth*, e2019JB019062.

Sichler, B. (1980). La biellette danakile: Un modèle pour l'évolution géodynamique de l'Afar. *Bulletin de la Société Géologique de France*, *22*(6), 925–932.

Smithsonian. (2023). *Volcanoes of the World (v. 5.0.2).* Retrieved 23 Jan 2023, from `https://doi.org/10.5479/si.GVP.VOTW5-2022.5.0`

Stephenson, S. N., Hoggard, M. J., Holdt, M. C., & White, N. (in review). Continental Residual Topography Extracted from Global Analysis of Crustal Structure.

Stephenson, S. N., White, N., Carter, A., Seward, D., Ball, P., & Klöcking, M. (2021). Cenozoic dynamic topography of Madagascar. *Geochemistry, Geophysics, Geosystems*, *22*(6), e2020GC009624.

Stuart, G., Bastow, I., & Ebinger, C. (2006). Crustal structure of the northern Main Ethiopian Rift from receiver function studies. *Geological Society, London, Special Publications*, *259*(1), 253–267.

Tesfaye, S., Harding, D. J., & Kusky, T. M. (2003). Early continental breakup boundary and migration of the Afar triple junction, ethiopia. *Geological Society of America Bulletin*, *115*(9), 1053–1067.

Thompson, D., Bastow, I., Helffrich, G., Kendall, J., Wookey, J., Snyder, D., & Eaton, D. (2010). Precambrian crustal evolution: seismic constraints from the Canadian Shield. *Earth and Planetary Science Letters*, *297*(3-4), 655–666.

Tiberi, C., Diament, M., Déverchère, J., Petit-Mariani, C., Mikhailov, V., Tikhotsky, S., & Achauer, U. (2003). Deep structure of the Baikal rift zone revealed by joint inversion of gravity and seismology. *Journal of Geophysical Research: Solid Earth*, *108*(B3).

Viltres, R., Jónsson, S., Ruch, J., Doubre, C., Reilinger, R., Floyd, M., & Ogubazghi, G. (2020). Kinematics and deformation of the southern Red Sea region from GPS observations. *Geophysical Journal International*, *221*(3), 2143–2154.

Watanabe, T. (1993). Effects of water and melt on seismic velocities and their application to characterization of seismic reflectors. *Geophysical Research Letters*,

20(24), 2933–2936.

Wessel, P., Luis, J., Uieda, L., Scharroo, R., Wobbe, F., Smith, W. H., & Tian, D. (2019). The generic mapping tools version 6. *Geochemistry, Geophysics, Geosystems*, *20*(11), 5556–5564.

White, R., & McKenzie, D. (1989). Magmatism at rift zones: the generation of volcanic continental margins and flood basalts. *Journal of Geophysical Research: Solid Earth*, *94*(B6), 7685–7729.

Wolfenden, E., Ebinger, C., Yirgu, G., Deino, A., & Ayalew, D. (2004). Evolution of the northern Main Ethiopian rift: birth of a triple junction. *Earth and Planetary Science Letters*, *224*(1-2), 213–228.

Wolfenden, E., Ebinger, C., Yirgu, G., Renne, P. R., & Kelley, S. P. (2005). Evolution of a volcanic rifted margin: Southern Red Sea, Ethiopia. *Geological Society of America Bulletin*, *117*(7-8), 846–864.

Zandt, G., & Ammon, C. J. (1995). Continental crust composition constrained by measurements of crustal Poisson's ratio. *Nature*, *374*(6518), 152–154.

Zelt, B., & Ellis, R. (1999). Receiver-function studies in the Trans-Hudson orogen, Saskatchewan. *Canadian Journal of Earth Sciences*, *36*(4), 585–603.

Zhu, L., & Kanamori, H. (2000). Moho depth variation in southern California from teleseismic receiver functions. *Journal of Geophysical Research: Solid Earth*, *105*(B2), 2969–2980.